

Planar Elliptic Broadband Antenna with Wide Range Reconfigurable Narrow Notched Bands for Multi-Standard Wireless Communication Devices

Imen Ben Trad¹, Jean Marie Floch¹, Hatem Rmili², *,
Lotfi Laadhar², and Mhamed Drissi¹

Abstract—A planar elliptic broadband antenna with reconfigurable dual stop-bands performance was successfully designed and performed for multi-standard wireless communication systems. The proposed antenna consists of a broadband micro-strip fed printed monopole operating in the frequency range 0.75–6 GHz. The notch-band characteristic was obtained by printing two Open Loop Resonators (OLRs) on the front side of the substrate close to the micro-strip feed-line. By adjusting the OLRs parameters, mono or dual band-rejection can be obtained. The passive broadband antenna was optimized to achieve narrow band rejection over the UMTS-band (around 2.1 GHz) and the WiMAX-band (around 3.5 GHz). The agility was produced by loading a varactor diode on each OLR. The major advantages of this structure are the high selectivity of the dismissed-bands, continuous reconfiguration and wide tuning range of the notched bands. Four prototypes were realized and experimentally characterized. The measured tuning ranges corresponding to the notched bands are about 850 MHz (2.25–3.1 GHz) for the rejected UMTS-band and 570 MHz (3.84–4.41 GHz) for the WiMAX-band. Simulated and measured results are presented and discussed.

1. INTRODUCTION

In recent years, wideband technology has been extensively investigated for wireless communication devices, and several applications were developed in which Wideband/Ultra Wideband (UWB) printed antennas were used due to their interesting properties as wide bandwidth, stable gain and radiation patterns in addition to their low cost and ease of fabrication and integration in PCB cards.

Despite these advantages, one main problem with this technology is the common use of wide frequency band by many wireless applications such as GSM, ISM, LTE, UMTS, WiFi, WLAN and WiMAX. This leads to a heavy congestion of the wireless spectrum, and the possibility of interferences and distortion of the transmitted electromagnetic signals.

However, the use of wideband antennas with notched-band characteristic may be a good alternative to avoid these constraints. In addition, by tuning the notched-bands, the developed antenna becomes a frequency reconfigurable structure which is more dynamic, flexible and suitable for several wireless applications. Actually, this intelligent solution has received a growing interest due to the increasing demand of multi-standards and smart antennas. In the literature, the frequency agility is typically provided by scaling the antenna dimensions electrically using several switching technologies such as PIN diodes, MEMS (Micro-Electro-Mechanical-Systems) switches and varactor diodes [4–9].

At the beginning, several rejected-band antennas were designed and successfully implemented, and parasitic elements and slots were used to realize mono/dual band-rejected compact and planar

Received 27 December 2013, Accepted 18 February 2014, Scheduled 25 February 2014

* Corresponding author: Hatem Rmili (hmrili@kau.edu.sa).

¹ IETR, INSA, 20 Avenue Buttes des Coësmes, Rennes 35043, France. ² Electrical and Computer Engineering Department, Faculty of Engineering, King Abdulaziz University, P. O. Box 80204, Jeddah 21589, Saudi Arabia.

antennas [1–3]. Next, the frequency reconfigurability was obtained by adding switches with different types [10–17]. For example, a reconfigurable stopband Vivaldi UWB antenna was realized by using two varactor diodes, but the notched-band was wide, and to narrow it, additional varactors and inductors were used which make the antenna structure more complex [10]. In [13], we have proposed a mono-band rejected broadband planar antenna with a wide tuning range of the discarded band by using only one varactor diode.

It is noteworthy that designing reconfigurable multi-notched bands antennas requires many switches which may increase the number of RF switches and then the complexity of the bias network. Consequently, the experimental characterization of an antenna with many switches will be a difficult task to be realized, which may explain for example the use of strips in [17] instead of the three PIN diodes required to achieve the frequency agility of a dual band-notched slot antenna.

In this perspective, a novel monopole broadband antenna with reconfigurable rejected dual-bands property is designed and presented in this paper. The major benefits of the proposed structure are the extremely selective and wide range tuning of notched bands. First, a planar elliptic broadband antenna was optimized and realized. Then two open loop resonators (OLRs) were printed on both edge sides of the micro-strip feed-line to discard two narrow bands. The targeted bands were the UMTS (2.1 GHz) and the WiMAX-bands (3.5 GHz). The frequency reconfigurable characteristic is obtained due to the integration of a varactor diode on each OLR element. The bias network related to the two varactor diodes is highly complex in practice. That's why only the two reconfigurable mono-rejected broadband antennas with single varactor were successfully designed and experimentally characterized to prove the concept, and to demonstrate that by electronically controlling each OLR, a local mismatch will be created without disturbing the antenna radiation. The reconfigurable rejected dual-bands antenna was only simulated.

2. ANTENNA DESIGN

The design procedure of the proposed antenna is realized in many steps. First, an elliptic-shaped patch (with major diameter $a = \lambda_{eff}/4$ at lower frequency and minor diameter b) and a feed-line ($L_f \times W_f$) were printed on the top layer of a Duroid substrate of length $L = 180$ mm, width = 160 mm, thickness $h = 0.8$ mm and permittivity $\epsilon_r = 2.2$ (Fig. 1(a)). Then, a rectangular-slot ($L_R \times W_R$) connected to a strip-slot ($L_s \times W_s$) was added to the elliptic-patch in order to improve the lower wideband frequency (Fig. 1(a)). Next, a partial ground plane ($L_g \times W$) was printed on the bottom side of the substrate (Fig. 1(b)). The main design parameters of the antenna were optimized for a good input impedance matching over the band 0.75–6 GHz (see Table 1).

To reach the band-rejection characteristic, two OLRs of dimensions $L_L \times W_L$, width e , gap W_1 and coupling distance d (from the feed-line) were added successively to the broadband antenna (A_1).

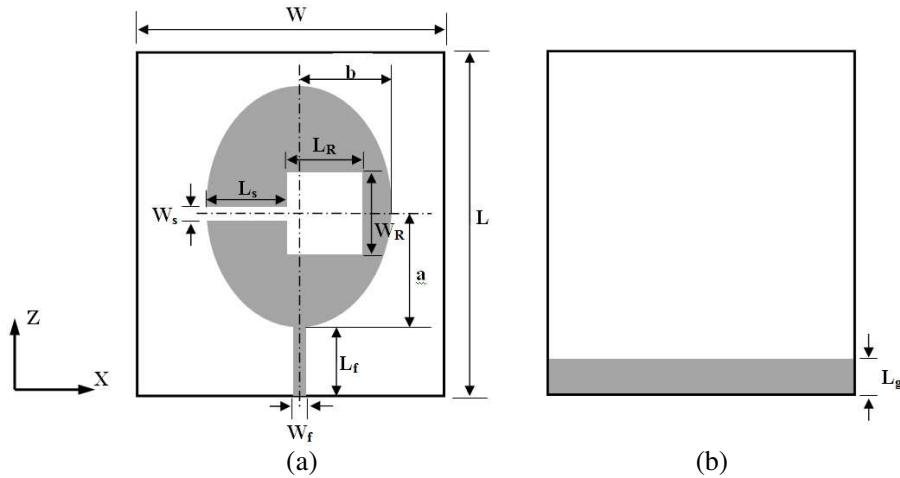


Figure 1. Schema of the elliptic broadband antenna A_1 : (a) top view; (b) bottom view.

Table 1. Design parameters of the antennas.

Patch (dimensions in mm)				OLR element (dimensions in mm)		
					A_2	A_3
a	75	L_s	50	L_L	18.55	11
b	50	l_R	40	W_L	9	7.8
L_f	20	w_R	40	e	1	1
W_f	2.2	L_g	19	W_1	1	1
W_s	4	W	160	d	0.5	0.2

Three configurations (see Fig. 2) were studied by considering one OLR or two OLRs. When the ORL element is placed on the left of the feed-line (antenna A_2) or on the right (antenna A_3), we obtain a mono-band rejection, whereas when both elements are considered, a dual-band rejection is obtained.

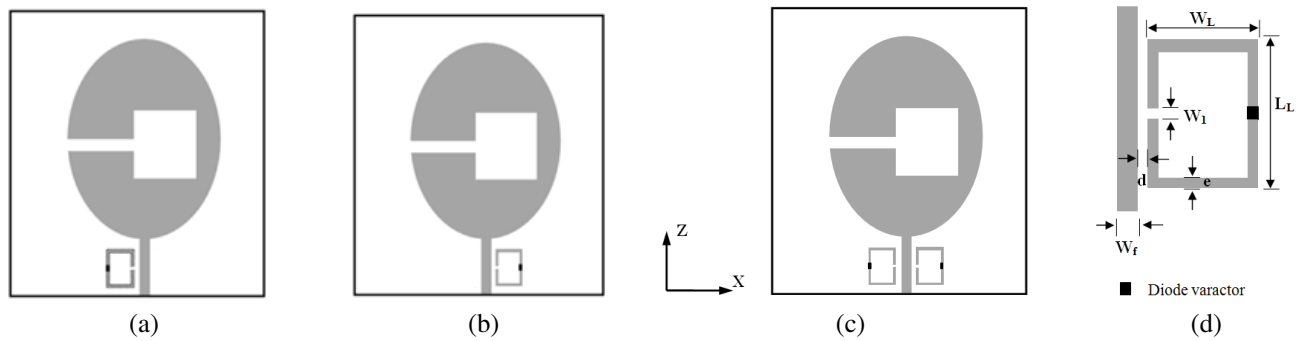


Figure 2. Schemas of the reconfigurable band-rejected antennas (top view): (a) OLR on the left (Antenna A_2); (b) OLR on the right (Antenna A_3); (c) antenna with the two OLRs (Antenna A_4); (d) geometry of the OLR element.

The mismatch created by integration of the OLRs is local and does not affect the antenna behaviour outside the notched bands. Besides, there is no correlation between the two OLRs behaviours; each resonator control one notched band independently on the other. The resonators were optimized in order to omit two narrow bands; the UMTS-band around 2.1 GHz and the WiMAX band around 3.5 GHz. Depending on the parasitic elements (OLRs) dimensions and the coupling distance, the first band was eliminated by the left integrated OLR, whereas the second one was eliminated due to the right OLR. The optimized design parameters of the studied antennas are resumed in Table 1. Finally, two SKYWORKS SMV1405 varactor diodes were loaded in the OLRs as shown in Fig. 2 for an electronically control and continuously tuning of the rejected bands over the wideband frequency.

3. RESULTS AND DISCUSSION

3.1. Simulations

The performances of the printed elliptic antennas including the rejected-band properties and the reconfigurable characteristics were investigated by using the electromagnetic simulator HFSS v13.

As can be seen from Fig. 3, antenna A_1 is able to achieve a wideband impedance matching ($|S_{11}| < -10$ dB) from 0.56 to 6 GHz. Return losses of the basic antenna A_1 with and without the rectangular slot are presented in order to prove the slot's effects. In fact, addition of the slot into the elliptic-shaped patch shifts the lower operating frequency by 440 MHz. The current path follows the shape of the slot as it can be remarked from Fig. 4, thus increasing the electric length of the patch and leading to better impedance matching at lower frequencies without increasing the physical dimensions.

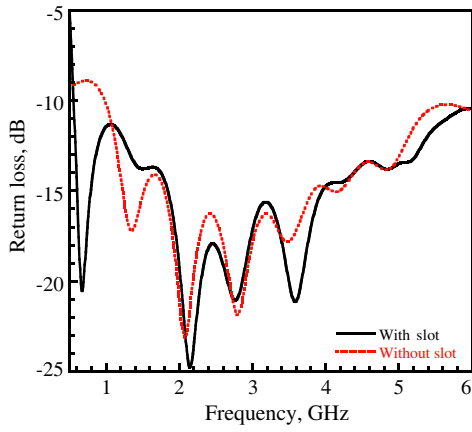


Figure 3. Return losses of the basic structure with and without slot.

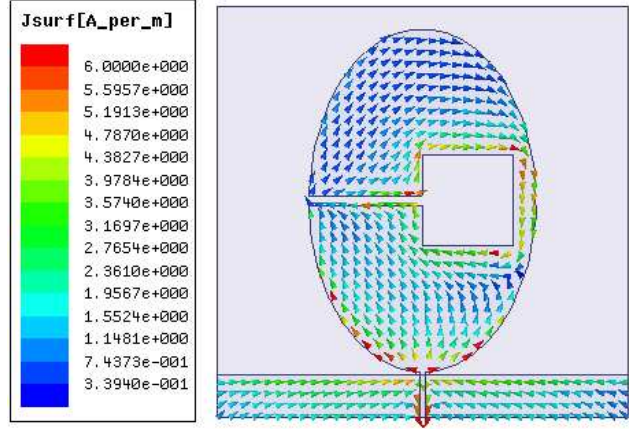
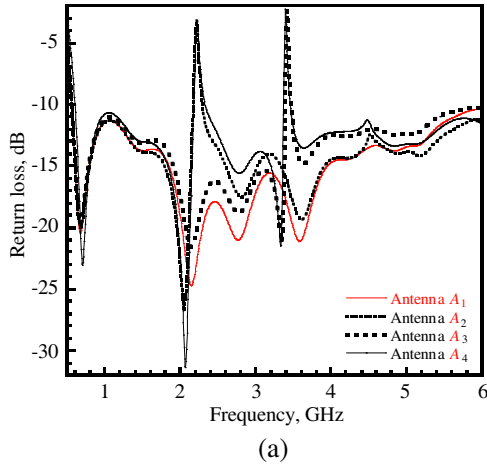
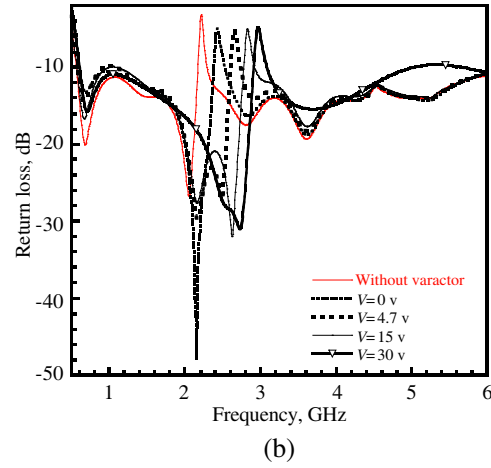


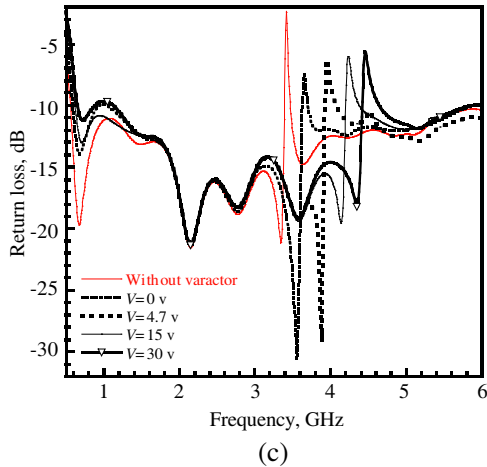
Figure 4. Vector current distribution at lower frequency $F = 0.56$ GHz.



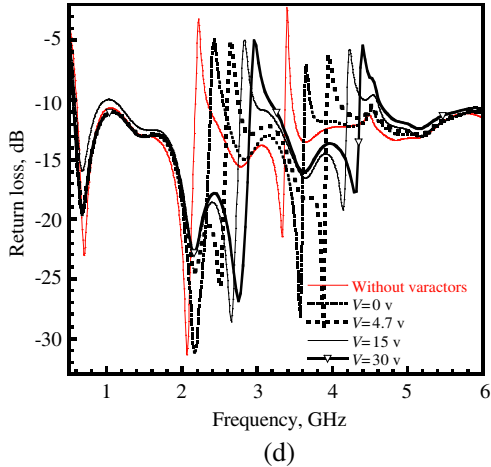
(a)



(b)



(c)



(d)

Figure 5. Simulated return loss of the: (a) four passive structures; (b) reconfigurable antenna A_2 ; (c) reconfigurable antenna A_3 , and (d) reconfigurable dual notched-bands antenna A_4 .

The simulated return losses of the basic structure A_1 , single rejected-band antennas A_2 and A_3 and dual rejected-bands antenna A_4 are depicted in Fig. 5(a). The rejection mechanism relies on the integration of parasitic OLRs on both sides of the micro-strip feed-line. Return losses of antennas A_2

and A_3 prove that each OLR is able to control one narrow notched band; it affects just the targeted frequencies of the UMTS- (for A_2) or the WiMAX-band (for A_3). When the two OLRs are printed (antenna A_4), both UMTS- and WiMAX-bands are omitted. The behaviour of antennas A_2 , A_3 and A_4 still unaltered outside targeted bands.

In fact, addition of the rectangular-shaped OLR element close to the micro-strip feeding line creates a magnetic coupling between the resonator and the feed-line, which causes a total reflection of the injected power at one selected frequency F_0 .

This notched frequency depends on the dimensions L_L and W_L of the OLR resonator as well as the coupling distance d , separating it from the feed-line.

At this frequency, the resonant current path L_{res} ($L_{res} \approx 2(L_L + W_L) - w_1$) in the OLR element corresponds to a half-wave length ($\lambda_{eff}/2$). λ_{eff} is the effective wavelength in the heterogeneous medium.

Then, the rejected frequency can be approximated by:

$$F_0 \approx \frac{c}{2\sqrt{\epsilon_{eff}}} \frac{1}{2(L_L + W_L) - w_1} \tag{1}$$

where c is the velocity of light in free space, and ϵ_{eff} the effective permittivity of the substrate.

A stop-band behavior appears around the resonant frequency of the OLR due to the negative magnetic permeability property of this structure, thus it acts as a band-stop filter while maintaining wideband performance from 0.56 to over 6 GHz.

In order to tune the notched-bands, we have loaded a varactor diode on each OLR element, which may change the effective length of the OLRs, and then its resonant frequency. The lumped element was modelled in simulations by considering a lumped capacitance C in series with a resistance R , where the different values of C and R were extracted from the data sheet of the components [18].

For reasons of clarity, only return losses corresponding to few values of C are presented. Table 2 summarizes the obtained rejected frequencies for all capacitance values (and their corresponding bias voltage) of active antennas A_2 , A_3 and A_4 . Fig. 5(b) and Fig 5(c) show the return losses of reconfigurable single notched-band antennas A_2 and A_3 . The narrow notched bands shift to higher frequencies while the wideband behaviour of the antennas still maintained. Antenna A_2 presents a simulated tuning range for its dismissed band of 700 MHz while antenna A_3 can achieve 600 MHz. The return loss of the dual rejected-bands antenna A_4 seems to be a superposition of the two return losses corresponding to mono rejected-band antennas A_2 and A_3 . This demonstrates that by controlling the electric length of each OLR element via its related varactor, the corresponding dismissed band will be continuously tuned in an independent way without disturbing the antenna radiation.

Table 2. Simulated rejected-frequencies of antennas A_2 , A_3 and A_4 for different capacitance values.

Capacitance value (pF)	Bias voltage (V)	A_2	A_3	A_4	
		Rejected frequency (GHz)	Rejected frequency (GHz)	Rejected frequency F_1 (GHz)	Rejected frequency F_2 (GHz)
Without varactor diode	–	2.1	3.5	2.1	3.5
$C = 2.81$	0	2.43	3.64	2.42	3.64
$C = 1.95$	1	2.5	3.75	2.5	3.75
$C = 1.19$	4.7	2.65	3.95	2.65	3.95
$C = 0.89$	10	2.76	4.1	2.76	4.08
$C = 0.75$	15	2.83	4.23	2.83	4.23
$C = 0.66$	20	2.88	4.32	2.88	4.3
$C = 0.56$	30	2.96	4.46	2.95	4.41

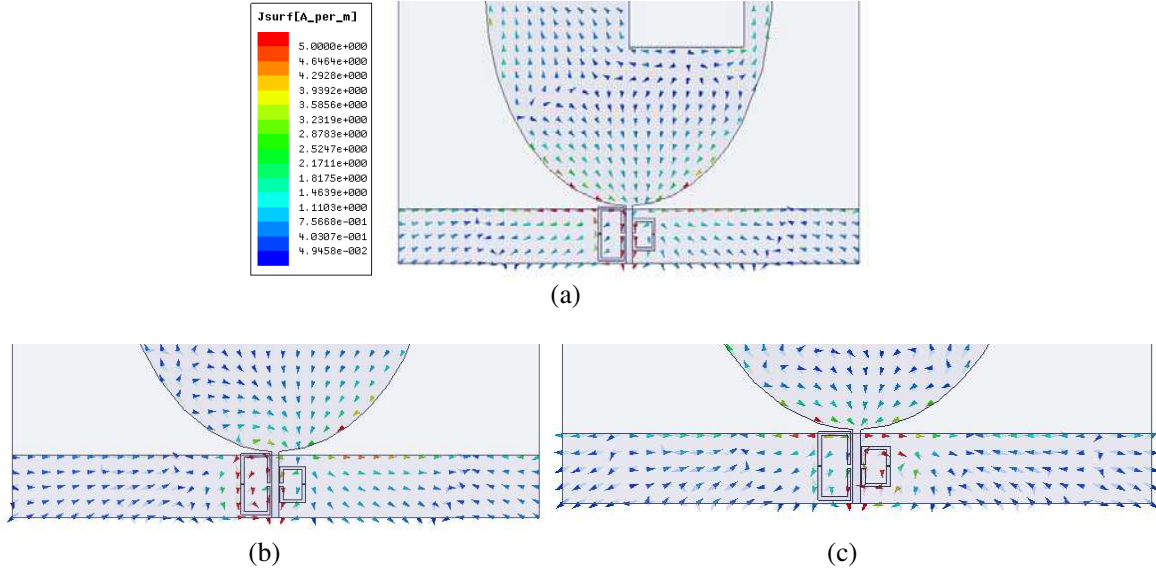


Figure 6. Vector current distribution of the proposed antenna A_4 for $C = 0.75$ pF at: (a) resonant frequency 2.65 GHz; (b) the lower dismissed frequency 2.83 GHz, and (c) the higher dismissed frequency 4.23 GHz.

To better analyze the designed structures, we have studied the surface current distribution in antenna A_4 for $C = 0.75$ pF ($V = 15$ v) (see Fig. 6). At the matched frequency 2.65 GHz, the currents are concentrated in the feed-line, edge sides of the elliptic patch and ground plane. The monopole radiation is not disturbed by the presence of the parasitic OLRs, it operates as predicted over the band 0.56–6 GHz outside the two notched bands. At the lower rejected frequency 2.83 GHz, which corresponds to the resonant frequency of the left OLR, only this element radiates causing total reflection of the injected power as it was expected. At the resonant frequency of the second OLR, only the right parasitic element (OLR) is activated thereby depriving the rest of the antenna of the injected power which allows the creation of the second rejected band as already explained above. We have verified by analyzing the surface current distribution in the structure that current paths in the ORL (left or right) and the feed-line are out of phase, which means that the resonances provided by negative permeable OLR elements were converted into anti-resonances (as needed for band-notch). The antenna band-notch behavior is then due mainly to current cancellation phenomena.

3.2. Measurements

The planar wideband antenna A_1 , the two reconfigurable mono band-rejected antennas A_2 and A_3 and their related bias networks and antenna A_4 (without tuning circuit) were successfully prototyped as shown in Fig. 7. Nevertheless, the integration of two varactor diodes on antenna A_4 is a hard task in practice because by increasing the number of varactors we increase also the complexity of the related bias network. For these reasons, only measurement results of antennas A_1 , A_2 , A_3 and A_4 (without varactor diodes) will be presented to prove the concept. Prototyped antennas were characterized by using the IETR Institute facilities. The return loss was measured by using the network analyzer Agilent N5230A over the frequency range 0.5–6 GHz. Measurements of gain and radiation patterns were carried out in the anechoic chamber “SATIMOSgate32”.

Simulated and measured return losses of the reference antenna A_1 are shown in Fig. 8(a) where a slight frequency shift can be noticed. The measured input impedance bandwidth 0.76–6 GHz exhibits a small disturbance at lower frequencies; this phenomenon was also noticed in [19]. In fact, in simulations, the coaxial connector model was not quite faithful to reality. It was approximated to a rectangular wave port to facilitate the design of the antenna using HFSS. This leads to think that the observed mismatch at lower frequencies may be assigned to the effect of the coaxial-connector feed. When the two OLRs

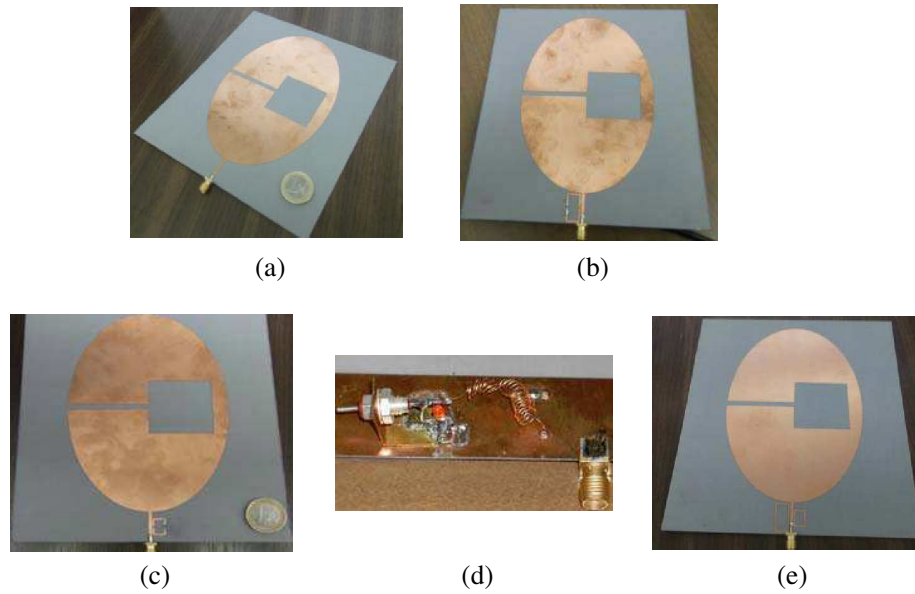


Figure 7. Photos of the realized prototypes: (a) broadband antenna A_1 (top view); (b) reconfigurable band-rejected antenna A_2 (top view); (c) reconfigurable band-rejected antenna A_3 (top view); (d) related bias network (bottom view), and (e) A_4 without varactor diodes.

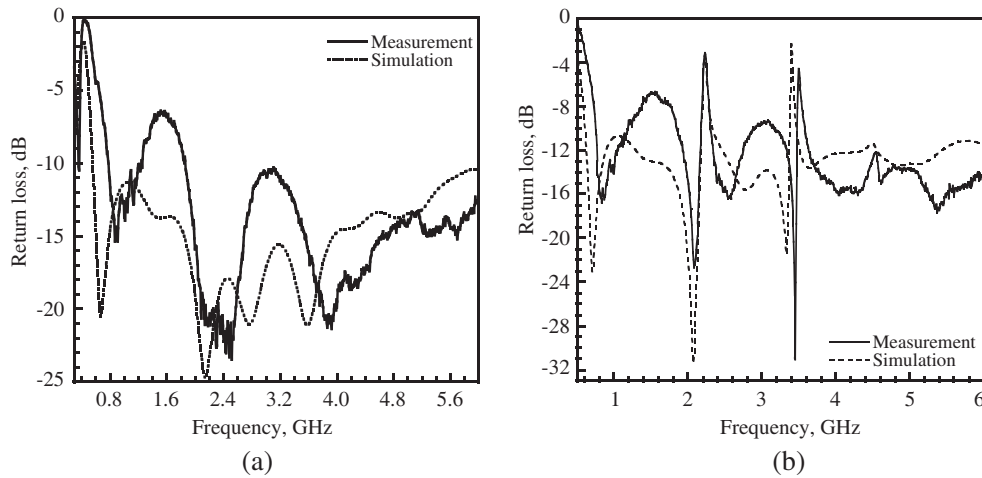


Figure 8. Measured and simulated return loss: (a) of the very wide band antenna A_1 and (b) of A_4 without varactor diodes.

are loaded, a local mismatch is created at resonant frequency of each OLR, hence creating the discarded UMTS- and WiMAX-bands. Measurements agree well with simulated results.

The measured return losses of antennas A_2 and A_3 are shown in Fig. 9 and Fig. 10, respectively. The varactor capacitance values, their corresponding measured notched-frequencies and notched bandwidths for both antennas are listed in Table 3. As it can be seen, the capacitance is inversely proportional to the applied reverse voltage. Therefore, as the capacitance value C decreases, reverse voltage increases and the narrow notched band shifts toward higher frequencies, and the wideband behavior of the antenna is maintained outside.

The monopoles can indeed preserve the reached wideband 0.75–6 GHz of the basic structure. For antenna A_2 , the achieved experimental tuning range of the dismissed band is from 2.4 to 3.1 GHz when a reverse voltage is applied on the varactor diode. This discarded band shifts to higher frequencies, whereas the application of a direct voltage (+0.5 V and +0.7 V) shifts the rejected band to lower frequencies and

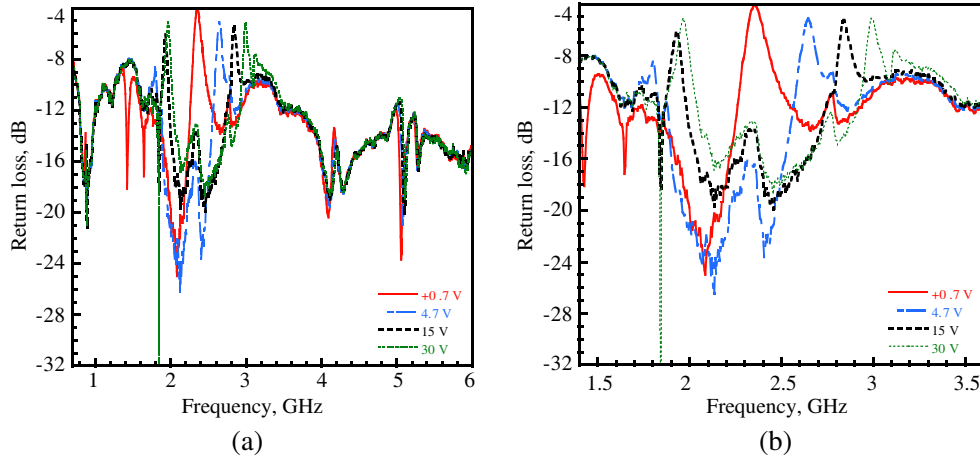


Figure 9. Measured return loss of the prototyped antenna A_2 : (a) over the operating band 0.75–6 GHz; (b) over 1.2–3.6 GHz band.

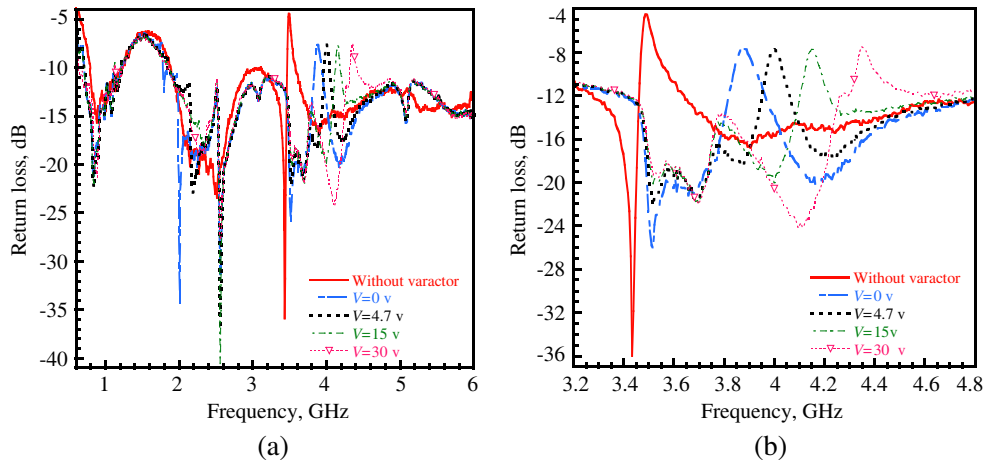


Figure 10. Measured return loss of the prototyped antenna A_3 : (a) over the operating band 0.75–6 GHz; (b) over 3.2–4.8 GHz band.

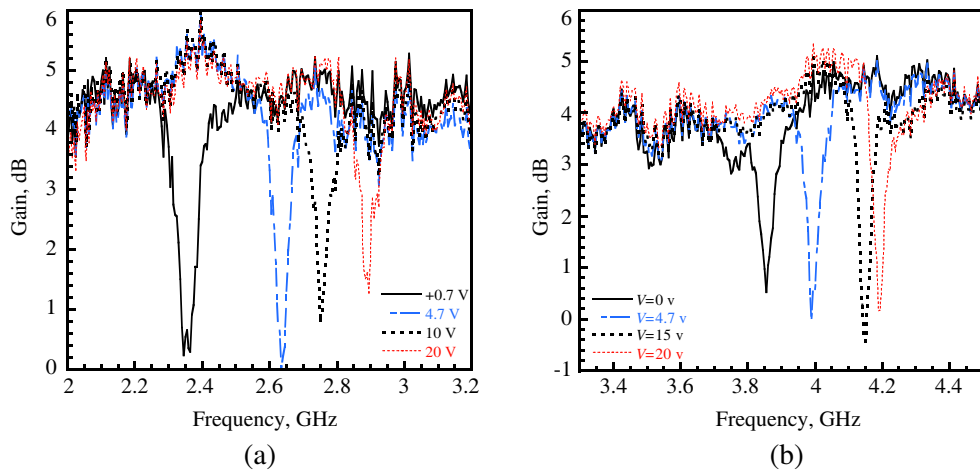


Figure 11. Measured gain of the reconfigurable structure for several values of the capacitance C : (a) antenna A_2 ; (b) antenna A_3 .

Table 3. Rejected-frequencies and their associated bandwidths of antennas A_1 and A_2 for different capacitance values.

Capacitance value (pF)	A_1			A_2		
	Bias voltage (V)	Rejected frequency (GHz)	Rejected bandwidth (MHz)	Bias voltage (V)	Rejected frequency (GHz)	Rejected bandwidth (MHz)
Without varactor diode	–	2.1	120	–	3.5	100
–	+0.7	2.35	190	–	–	–
–	+0.5	2.42	190	–	–	–
$C = 2.81$	0	2.46	170	0	3.87	90
$C = 1.95$	1	2.51	170	1	3.89	90
$C = 1.19$	4.7	2.64	160	4.7	3.99	70
$C = 0.89$	10	2.76	140	10	4.084	70
$C = 0.75$	15	2.84	160	15	4.149	70
$C = 0.66$	20	2.88	210	20	4.199	70
$C = 0.56$	30	2.98	140	30	4.344	90

offers a supplement tuning range of 150 MHz. Hence, a total tuning range of 850 MHz is easily achieved (Fig. 9). The bandwidth related to the OLR alone is about 300 MHz; this value decreases when it is associated to the antenna as it can be concluded from Table 3.

Otherwise, a frequency agility of 570 MHz for antenna A_3 is also obtained (from 3.84 to 4.41 GHz). The measured return loss of the structure without varactor diode is presented as reference in Fig. 10.

We note the presence of slight differences between simulated and measured omitted frequencies because of the small discrepancies between the real diodes and their models used in simulation.

The measured gain of antennas A_2 and A_3 for several values of the varactor diode capacitance C are presented in Fig. 11. The assessment of the measured gain curves dealing with the frequency reconfigurable antennas shows a drop at the notched bands, a local mismatch is caused by the

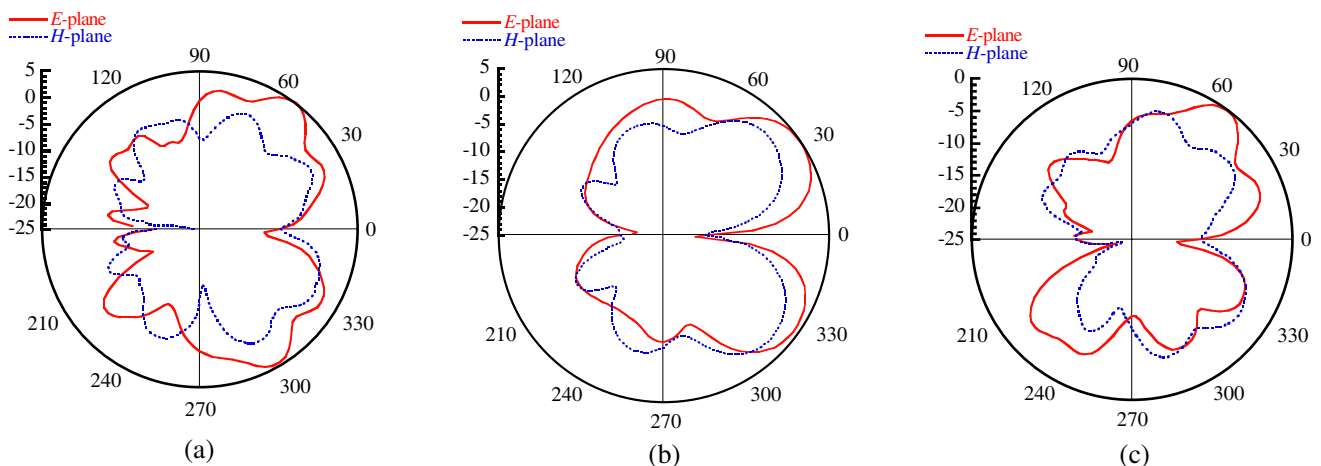


Figure 12. Measured radiation patterns for: (a) antenna A_1 at 4 GHz; (b) antenna A_4 at 2.1 GHz, and (c) 3.5 GHz (without varactors).

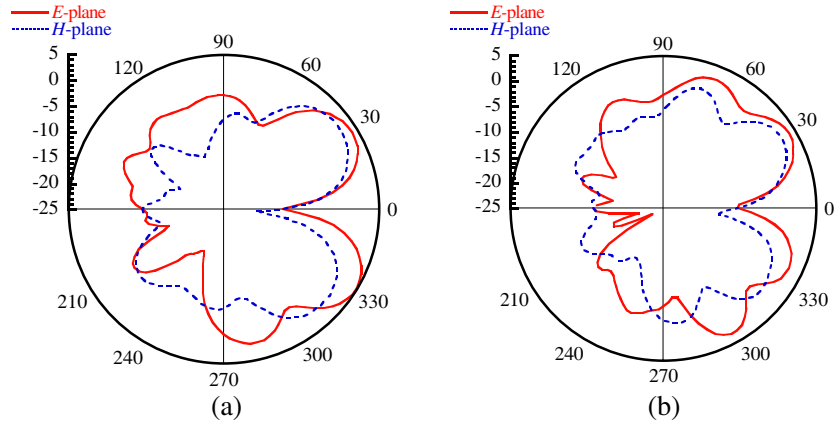


Figure 13. Measured radiation patterns for the reconfigurable antenna A_2 for $C = 0.75$ pF (15 V) at frequencies: (a) 2.45 GHz and (b) 3.2 GHz.

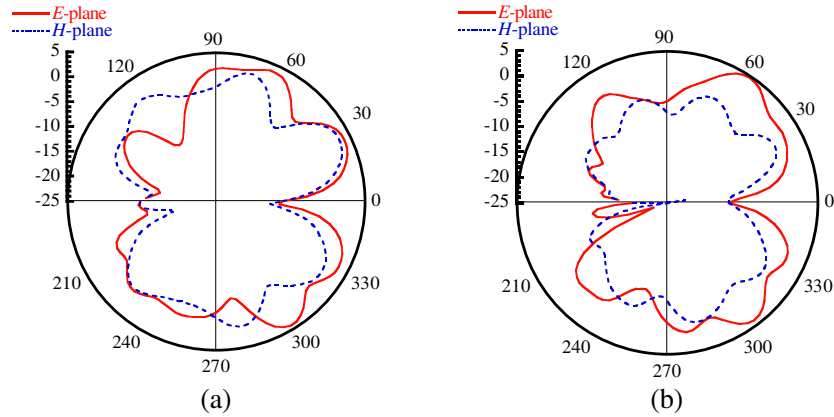


Figure 14. Measured radiation patterns for the reconfigurable antenna A_3 for $C = 0.75$ pF at frequencies: (a) 3.4 GHz and (b) 4 GHz.

open loop. Actually, the gain decreases drastically at the vicinity of the loop's resonant frequency bands while preserving the same performances outside. The measured gain attests that a frequency notch reconfiguration is clearly achieved using the varactor diode. The significant gain drop for each capacitance value C is slightly different and can be deteriorated at higher frequencies (beyond $C = 0.66$ pF) especially for A_2 .

Figures 12–14 exhibit measured radiation patterns of the wideband antenna A_1 , antenna A_4 (without varactors) and antennas A_2 and A_3 in both E -plane ($yo z$) and H -plane ($xo z$) at selected frequencies for $C = 0.75$ pF (15 V). A stable radiation pattern is almost achieved and is well maintained over the whole operating broadband 0.76–6 GHz. It can be concluded that the reconfigurable OLR elements eliminate the undesired bands without contributing to the antenna's radiation.

4. CONCLUSION

In this paper, a new broadband planar antenna, with frequency reconfigurable notched-bands, is designed for band rejection of the UMTS- (2.1 GHz) or/and the WiMAX-bands (3.5 GHz).

The electronic control of the discarded bands over the broadband frequencies was obtained by loading varactor diodes which permits to obtain the desired rejected-bands while maintaining good impedance matching and radiation properties outside. Two mono notched-band antennas with only one varactor diode were designed, simulated, realized and experimentally characterized, whereas the dual

notched-band antenna was only simulated due to the complexity of the required bias network.

The developed active antenna with its selective and wide range tuning of notched bands, monopole-like patterns, stable radiation properties, and moderate gain may be a potential structure for wireless applications.

ACKNOWLEDGMENT

This work was funded by the Deanship of Scientific Research (DSR), King Abdulaziz University, Jeddah, under grant No. 135-015-D1434. The authors, therefore, acknowledge with thanks DSR technical and financial support.

Special thanks to Mr. Laurent DESCLOS from Ethertronics at San Diego US, for his help to finalize this work.

REFERENCES

1. Choi, N., C. Jung, J. Byun, F. J. Harackiewicz, M.-J. Park, Y.-S. Chung, T. Kim, and B. Lee, "Compact UWB antenna with I-shaped band-notch parasitic element for laptop applications," *IEEE Antennas and Wireless Propagation Letters*, Vol. 8, 580–582, 2009.
2. Ben Trad, I., H. Rmili, J. M. Floc'h, and H. Zangar, "Design of planar mono-band rejected UWB CPW-fed antennas for wireless communications," *Mediterranean Microwave Symposium, MMS Proceeding*, 175–178, 2011.
3. Ben Trad, I., H. Rmili, J. M. Floc'h, and H. Zangar, "Design of a dual-band rejected UWB printed monopole antenna," *EuCAP Proceeding*, 651–654, 2011.
4. Canneva, F., F. Ferrero, J. M. Ribero, and R. Staraj, "Reconfigurable miniature antenna for DVB-H standard," *IEEE Antenna and Propagation Society International Symposium (APSURSI)*, 1–4, 2010.
5. Lee, M.-J., Y.-S. Kim, and Y. Sung, "Frequency reconfigurable planar inverted-F antenna (PIFA) for cell-phone applications," *Progress In Electromagnetics Research C*, Vol. 32, 27–41, 2012.
6. Ren, Z., W. Li, L. Xu, and X. Shi, "A compact frequency reconfigurable unequal U-slot antenna with a wide tunability range," *Progress In Electromagnetics Research Letters*, Vol. 39, 9–16, 2013.
7. Aka, M., C. Niamien, A. Sharaiha, S. Collardey, and K. Mahdjoubi, "An electrically small frequency reconfigurable antenna for DVB-H," *IEEE International Workshop on Antenna Technology*, 245–248, 2012.
8. Cai, Y., Y. J. Guo, and T. S. Bird, "A frequency reconfigurable printed Yagi-Uda dipole antenna for cognitive radio applications," *IEEE Transactions on Antennas and Propagation*, Vol. 60, No. 6, 2905–2912, Jun. 2012.
9. Lee, S. W., Y. Sung, J. Y. Park, S. J. Lee, and B. J. Hur, "Frequency reconfigurable antenna using a PIN diode for mobile handset application," *EuCAP Proceeding*, 2053–2054, 2013.
10. Artiga, X., J. Perruisseau-Carrier, P. Pardo-Carrera, I. Llamas-Garro, and Z. Brito-Brito, "Design of Vivaldi antennas with embedded reconfigurable stopband filter," *EuCAP Proceeding*, 2284–2288, 2011.
11. Perruisseau-Carrier, J., P. Pardo-Carrera, and P. Miskovsky, "Modeling, design and characterization of a very wideband slot antenna with reconfigurable band rejection," *IEEE Transactions on Antennas and Propagation*, Vol. 58, No. 7, Jul. 2010.
12. Ojaroudi, M., G. Ghanbari, N. Ojaroudi, and C. Ghobadi, "Small square monopole antenna for UWB applications with variable frequency band-notch function," *IEEE Antennas and Wireless Propagation Letters*, Vol. 8, 1061–1064, 2009.
13. Ben Trad, I., J. M. Floc'h, H. Rmili, M. Drissi, and H. Zangar, "Design of a planar reconfigurable band-rejected UWB antenna for multi-standard wireless communication systems," *2012 Loughborough Antennas and Propagation Conference (LAPC)*, 1–4, 2012.
14. Hamid, M. R., P. Gardner, P. S. Halland, and F. Ghanem, "Reconfigurable vivaldi antenna with tunable stop bands," *IEEE International Workshop on Antenna Technology*, 54–57, 2011.

15. Kalteh, A. A., G. R. Dadash Zadeh, M. Naser-Moghadasi, and B. S. Virdee, "Ultra-wideband circular slot antenna with reconfigurable notch band function," *IET Microwaves, Antennas & Propagation*, Vol. 6, No. 1, 108–112, 2012.
16. Nikolaou, S., N. D. Kingsley, G. E. Ponchak, J. Papapolymerou, and M. M. Tentzeris, "UWB elliptical monopoles with a reconfigurable band notch using MEMS switches actuated without bias lines," *IEEE Transactions on Antennas and Propagation*, Vol. 57, No. 8, Jul. 2009.
17. Li, Y., W. Li, and Q. Ye, "A CPW-fed circular wide-slot UWB antenna with wide tunable and flexible reconfigurable dual notch bands," *The Scientific World Journal*, Vol. 2013, Article ID 402914, <http://dx.doi.org/10.1155/2013/402914>, 2013.
18. <http://datasheet.octopart.com/SMV1405-040LF-Skyworks-Solutions-datasheet-11039839.pdf>.
19. Ben Trad, I., H. Rmili, J.-M. Floc'h, and H. Zangar, "Design of a dual-band rejected UWB printed monopole antenna," *European Conference on Antennas and Propagation (EuCAP) Proceeding*, 651–654, 2011.